IEEE Access
Multidisciplinary ⋮ Rapid Review ⋮ Open Access Journal

Received 9 July 2023, accepted 23 July 2023, date of publication 2 August 2023, date of current version 9 August 2023.

Digital Object Identifier 10.1109/ACCESS.2023.3301147

RESEARCH ARTICLE

Anti-Disturbance Tracking Control for a Class of PMSM Driven-Based Flexible Manipulator Systems With Input Saturation and Angular Velocity Constraint

WENYE ZHOU, CHEN LIN, AND YANG YI
College of Information Engineering, Yangzhou University, Yangzhou 225127, China

Corresponding author: Yang Yi (yiyang@yzu.edu.cn)

This work was supported in part by NSFC under Grant 61973266, in part by the Foundation of Key Laboratory of National Defense Science and Technology under Grant JSY6142219202115, and in part by the Project of Xuzhou Key Research and Development under Grant KC21080.

ABSTRACT This paper proposes a feasible anti-disturbance constrained control algorithm for a class of typical permanent magnet synchronous motor (PMSM) driven-based single-joint flexible manipulator systems with input saturation and angular velocity constraint. Firstly, by actuating with a surface-mounted PMSM, and setting the d-axis current as zero, the single-joint flexible manipulator is converted into a normal state space model. Secondly, compared with classical harmonic or linear disturbance, the exogenous disturbance model with configurable parameters and the associated disturbance observer (DO) are continuously introduced to dynamically estimate those unknown irregular disturbance. Moreover, by combining the convex hull representation of the saturating input with the suggested adaptive law, an efficient adaptive active anti-disturbance controller is designed to ensure the stability of closed-loop manipulator systems. By using convex optimization technique, not only the dynamic tracking for the rotation position but also the angular velocity constraint can be guaranteed simultaneously. Finally, simulation results for three different kinds of disturbances are showed to demonstrate the superiority of the proposed method.

INDEX TERMS Anti-disturbance control, single-joint flexible manipulators, disturbance observer (DO), permanent magnet synchronous motor (PMSM), input saturation.

I. INTRODUCTION

For the past few years, flexible manipulator systems have increasingly become an indispensable part of the automation industry, such as intelligent manufacturing, aerospace, medical industry, and so on [1], [2], [3], [4]. Compared with generic rigid mechanical arms [5], [6], flexible manipulators have the superiorities of lower energy consumption, higher safety, lighter structure, and stronger adaptability in the environment. However, most early results of manipulator control are only focused on the open-loop control method. In the process of control, the design and function of the driver are also often ignored [7], [8]. PMSMs are commonly used as the driving equipment for robotic manipulator servo control due to their high power factor, strong starting torque, and highly efficient properties [9], [10]. Nowadays, the attitude control issue of flexible manipulator systems driven by PMSM is becoming increasingly prominent in modern society [11], [12]. In [11], in order to achieve precise trajectory tracking and position monitoring, a nonlinear controller integrating adaptive Kalman filter load torque observer with neural networks (NNs) was presented for the n-joint robot system powered by PMSM. The famous H_∞ and L_2/L_∞ methods were introduced to recede the influences of the disturbances existing in an uncertain flexible manipulator system [12]. However, during the movement of the manipulator, it is inevitable to suffer from irregular disturbances and state constraints, including input saturation and upper

The associate editor coordinating the review of this manuscript and approving it for publication was Jinquan Xu.

bound on angular velocity, which makes controller design more complicated. How to explore a simple and feasible anti-disturbance algorithm with different constraints is still an open problem.

In the field of automatic control, the theory of anti-disturbance control has received extensive attention in recent years. Many advanced anti-interference methods have been proposed to suppress or attenuate the effects of different types of disturbance, including H_∞ control [13], adaptive control [14], output regulation theory [15] and disturbance-observer-based control (DOBC) [16], [17]. Among them, the DOBC method proposed in the 1980s is widely used in linear and nonlinear systems [16]. As a kind of active anti-disturbance method with a simple structure and easy to implement, DOBC has been successfully applied to different controlled systems and realized favorable anti-disturbance performance. For example, stochastic jump systems, multi-agent systems, and aerial vehicle systems. Notably, the DOBC technique typically requires information on the frequency and amplitude of unidentified disturbances, making it simple to estimate and solve linear or regular disturbances, such as harmonic and constant disturbances [17]. When influenced by those nonlinear irregular disturbances, the pre-existing disturbances modeling and estimation techniques will be invalid. Thus, exploring more effective disturbance modeling tools and methods is very important. Dynamical neural networks (DNNs) have better memory capabilities than other NN models, which allows them to be especially well-suited for modeling those irregular dynamics [18], [19], [20]. In [20], by conducting the exogenous DNN disturbance models, a DOB adaptive control technique with configurable parameters is proposed to achieve dynamical estimation and attenuation of irregular disturbances.

As we all know, during the manipulator operation, the phenomenon of constraints can not be avoided. In nonlinear constraints, actuator saturation can weaken almost all control equipment and severely degrade system performance [21], [22]. In response to this issue, many scholars began to study saturation actuator control systems to create effective saturation control algorithms [22], [23], [24]. In [22], the hyperbolic tangent function and the Nussbaum function are applied to eliminate the nonlinear term resulting from input saturation. It has also been suggested to employ bilinear matrix inequalities (BLMIs) or linear matrix inequalities (LMIs) strategy to implement the polytopic techniques for compressing saturation functions into convex packages [23], [24]. Another typical constraint is the state constraint problem, for example, the upper bound constraint of angular velocity in flexible manipulator systems. In light of this, a variety of solutions to work out the state constraint problem have been put forward, including model predictive control [25], reference governor [26], barrier Lyapunov functions (BLFs) [27] and so on. However, when simultaneously facing saturating actuator, state constraints, as well as different types of disturbances, different degrees of couplings are bound to occur. Under such circumstances, it is worth further studying to find an effective controller with the requirement for multiple objectives.

The aforementioned research served as the inspiration for this paper. An effective DOB anti-disturbance tracking control is considered for PMSM-driven flexible manipulator systems with input saturation, unidentified disturbances, as well as rotational velocity constraints. The proposed scheme has the following characteristics. (i) By importing the exogenous disturbance model with adjustable parameters, a new DO algorithm with adaptive law is proposed to realize the dynamical estimation of irregular disturbances. In contrast with linear or harmonic disturbances in [28] and [29], the adaptive DO strategy broadens the variety of applications for disturbances. (ii) By using the convex hull representation of the saturating input, the coupling issue in the control port is successfully resolved. Then, an effective anti-disturbance anti-windup controller can also developed along with the estimate of unknown disturbances. (iii) Further, based on the designed optimization algorithm, the multiple objective requirements, including stability, robustness, dynamic tracking for the rotation position, and the angular velocity constraint, can be successfully realized. (iv) By modeling different attenuated harmonic (AH), irregular triangular wave (ITW), and white noise (WN) disturbances, respectively, the simulation results for a single-joint flexible manipulator are shown to demonstrate the viability of the suggested control algorithm.

Nomenclature. In this paper, $\mathbf{0}$ and $\mathbf{I}$ stand in for the zero and identity matrices. With regard to a matrix $\circ$, the symbol sym is described by $sym(\circ) = \circ + \circ^T$.

II. DESCRIPTION OF SINGLE-JOINT FLEXIBLE MANIPULATOR ACTUATED BY PMSM

Consider the single-joint manipulator system actuated by a surface-mounted PMSM, and the concrete form is described as

$$\begin{cases} F\ddot{q} + H\dot{q} + G(q) = K(q - q_m) \\ J\ddot{q}_m + K(q_m - q) = l_p\psi i_q \\ L_s\dot{i}_d + R_s i_d - l_p\dot{q}_m L_s i_q = \mathbf{sat}\,(u_d + \sigma_1(t)) \\ L_s\dot{i}_q + R_s i_q + l_p\dot{q}_m L_s i_d + l_p\psi\dot{q}_m = \mathbf{sat}\left(u_q + \sigma_2(t)\right) \end{cases} \tag{1}$$

where q, $\dot{q}$, and $\ddot{q}$ are the rotation position, the rotation angular velocity, and the angular acceleration of the joint. q_m, $\dot{q}_m$, and $\ddot{q}_m$ stand for the motor rotation angle, angular speed vectors, and rotation angular acceleration separately. u_d, u_q, i_d and i_q are the stator voltages and the currents of d and q-axes. Note that $\mathbf{sat}(\star)$ stands for a saturation function with $\mathbf{sat}(\star) = [sat_1(\star), sat_2(\star), \cdots, sat_s(\star)]$, where $sat_i(\star) = sign(\star)min\{1, \star\}$ with the signum function $sign(\star)$. F, H, and $G(q) = Mglsin(q)$ represent the moment of inertia, the viscous frictional coefficient, and the gravity vector, respectively. J and K represent the motor rotational inertia and the spring elasticity coefficient, and both are positive constants. l_p is the number of pole pairs. L_s and R_s are the inductance and resistance of a stator, ψ is the linkage for rotor flux. $\sigma_i(t)$, $i = 1, 2$ are unknown exogenous disturbances.

In this case, the reference value of the d-axis current i_d^* is set to zero in order to obtain the highest torque-to-current ratio. If the controller of i_d loop works well, one obtains $\dot{i}_d = \dot{i}_d^* = 0$. In such a case, system (1) can be reduced as

$$\begin{cases} F\ddot{q} + H\dot{q} + G(q)K(q - q_m) \\ J\ddot{q}_m + K(q_m - q) = l_p\psi i_q \\ L_s\dot{i}_q + R_s i_q + l_p\psi\dot{q}_m = \mathbf{sat}\left(u_q + \sigma_2(t)\right) \end{cases} \tag{2}$$

Further, by defining $x_1 = q, x_2 = \dot{q}, x_3 = q_m, x_4 = \dot{q}_m$ and $x_5 = i_q$, the flexible manipulator system (2) is rewritten as

$$\begin{cases} \dot{x}_1 = x_2 \\ \dot{x}_2 = \dfrac{1}{F}\left[K\left(x_3 - x_1\right) - Mglsin(x_1) - Hx_2\right] \\ \dot{x}_3 = x_4 \\ \dot{x}_4 = \dfrac{K}{J}\left(x_1 - x_3\right) + \dfrac{l_p}{J}\psi x_5 \\ \dot{x}_5 = \dfrac{1}{L_s}\left[-R_s x_5 - l_p\psi x_4 + \mathbf{sat}\left(u_q + \sigma_2(t)\right)\right] \end{cases} \tag{3}$$

Suppose $x(t) = [x_1, x_2, x_3, x_4, x_5]^T$, then the system (3) is described by the state-space model, that is

$$\begin{cases} \dot{x}(t) = \mathcal{A}x(t) + \mathcal{B}\mathbf{sat}\left(u_q(t) + \sigma_2(t)\right) + \mathcal{C}h(x(t), t) \\ y(t) = \mathcal{D}x(t) \end{cases} \tag{4}$$

with

$$\mathcal{A} = \begin{bmatrix} 0 & 1 & 0 & 0 & 0 \\ -\dfrac{K}{F} & -\dfrac{H}{F} & \dfrac{K}{F} & 0 & 0 \\ 0 & 0 & 0 & 1 & 0 \\ \dfrac{K}{J} & 0 & -\dfrac{K}{J} & 0 & \dfrac{l_p}{J}\psi \\ 0 & 0 & 0 & -l_p\psi & -\dfrac{R_s}{L} \end{bmatrix}$$

$$\mathcal{B} = \begin{bmatrix} 0 \\ 0 \\ 0 \\ 0 \\ \dfrac{1}{L} \end{bmatrix}, \mathcal{C} = \begin{bmatrix} 0 \\ \dfrac{1}{F} \\ 0 \\ 0 \\ 0 \end{bmatrix}, \quad \mathcal{D}^T = \begin{bmatrix} 1 \\ 0 \\ 0 \\ 0 \\ 0 \end{bmatrix}$$

where $x(t) \in \mathbb{R}^{5\times 1}$, $\sigma_2(t)$, $u_q(t)$ and $y(t) \in \mathbb{R}^{5\times 1}$ denote the state vector, the unknown disturbance, the controlled input, and the system output, respectively. The constant matrices $\mathcal{A}$, $\mathcal{B}$, $\mathcal{C}$, and $\mathcal{D}$ as well as the nonlinear expression $h(x(t), t) = -Mglsin(x_1)$ are known.

To better estimate unknown disturbances, $\sigma_2(t)$ is assumed to be described by an exogenous model with adjustable parameters as

$$\begin{cases} \dot{\epsilon}(t) = M_1\epsilon(t) + \aleph^*\Psi(\epsilon(t)) \\ \sigma_2(t) = M_2\epsilon(t) \end{cases} \tag{5}$$

where $\epsilon(t) \in \mathbb{R}^5$ is the middle state of the disturbance model, and M_1 and M_2 are known coefficient matrices. Besides, $\aleph^* \in \mathbb{R}^{5\times 5}$ is the optimal parameter matrix, and $\Psi(\star)$ is the activation function with $\Psi(\star) = [\phi_1(\star), \ldots, \phi_5(\star)]^T$. By selecting different activation functions and adjusting dynamical weights, the model (5) can be a useful identifier to depict different types of disturbances.

Remark 1: It is necessary to note that nonlinear disturbances often occur in practical engineering, including attenuated harmonic disturbances, irregular triangular wave disturbance, white noise disturbances, and so on. In this case, it is essential to per-select the appropriate activation function $\Psi(\epsilon(t))$. According to the properties and characteristics of DNNs, the above DNN interference model can approximately describe any type of exogenous disturbances as long as a suitable activation basis function is found. The detailed discussion of this can also be presented in the simulation example in Section V.

For further discussing the above multi-objective task, an extended state variable is defined as

$$\bar{\chi}(t) = \left[x^T(t), \int_0^t e^T(\tau)d\tau\right]^T \tag{6}$$

where y_d represents the anticipated output and $e(t) := y(t) - y_d$ defines the tracking error. According (4) with (6), the extended system can be expressed by

$$\begin{cases} \dot{\bar{\chi}}(t) = \mathcal{A}^*\bar{\chi}(t) + \mathcal{B}^*\mathbf{sat}\left(u_q(t) + \sigma_2(t)\right) \\ \qquad\qquad +\mathcal{C}^*\tilde{h}\left(\bar{\chi}(t), t\right) + \bar{\mathcal{C}}y_d \\ y(t) = \mathcal{D}^*\bar{\chi}(t) \end{cases} \tag{7}$$

where

$$\mathcal{A}^* = \begin{bmatrix} \mathcal{A} & 0 \\ \mathcal{D} & 0 \end{bmatrix}, \mathcal{B}^* = \begin{bmatrix} \mathcal{B} \\ 0 \end{bmatrix}, \mathcal{C}^* = \begin{bmatrix} \mathcal{C} \\ 0 \end{bmatrix}, \bar{\mathcal{C}} = \begin{bmatrix} 0 \\ -I \end{bmatrix}$$

and $h(x(t), t) = \tilde{h}(\bar{\chi}(t), t) = -Mglsin(x_1)$. The derivative of $\tilde{h}(\bar{\chi}(t), t)$ with regard to x_1 can easily be inferred to be bounded. Moreover, the nonlinear function $\tilde{h}(\bar{\chi}(t), t)$ can be assumed to satisfy the bounded condition described as Lipschitz form. For any $\bar{\mathbf{x}}_j(t) \in \mathbb{R}^{5\times 1}, j = 1, 2$, the nonlinear function $\tilde{h}(\bar{\chi}(t), t)$ satisfies

$$\begin{cases} \tilde{h}(0, t) = 0 \\ ||\tilde{h}(\bar{\mathbf{x}}_1(t), t) - \tilde{h}(\bar{\mathbf{x}}_2(t), t)|| \le ||\Pi(\bar{\mathbf{x}}_1(t) - \bar{\mathbf{x}}_2(t))|| \end{cases} \tag{8}$$

where Π is a given constant weighting matrix.

III. DESIGN OF DISTURBANCE OBSERVER AND ANTI-DISTURBANCE CONTROLLER

This section proposes a nonlinear DO with adjustable weights for dynamic estimation of the $\sigma_2(t)$, where the corresponding form is

$$\begin{cases} \hat{\sigma}_2(t) = M_2\hat{\epsilon}(t) \\ \hat{\epsilon}(t) = \xi(t) - M_2\bar{\chi}(t) \\ \dot{\xi}(t) = \left(M_1 + \mathbf{L}\mathcal{B}^*M_2\right)\left(\xi(t) - \mathbf{L}\bar{\chi}(t)\right) + \mathbf{L}\left(\mathcal{A}^*\bar{\chi}(t)\right. \\ \qquad \left. + \mathcal{B}^*u_q(t) + \mathcal{C}^*\tilde{h}(\bar{\chi}(t), t) + \bar{\mathcal{C}}y_d\right) - \hat{\aleph}(t)\Psi(\hat{\epsilon}(t)) \end{cases} \tag{9}$$

where $\xi(t)$ stands for the subsidiary variable, $\hat{\aleph}(t)$ is the adjustable weight, $\hat{\sigma}_2(t)$ represents the estimate of $\sigma_2(t)$, $\mathbf{L}$ is the observer gain.

The composite controller is created with the dynamical estimation of the disturbance as

$$u(t) = \mathbf{K}\bar{\chi}(t) - \hat{\sigma}_2(t), \mathbf{K} = [\mathbf{K}_P, \mathbf{K}_I] \tag{10}$$

where $\mathbf{K}_P$ and $\mathbf{K}_I$ represent desired controller gains.

By using the polytopic bounding method, and selecting $G = [G_1, M_2]$ such that $\varrho(t) \in \mathbf{L}(G)$, the saturated input term can be deduced as

$$\begin{aligned} sat\left(u_q + \sigma_2\right) &= \sum_{i=1}^{2} \vartheta_i \left(\Xi_i[\mathbf{K}, M_2]\varrho(t) + \Xi_i^- G\varrho(t)\right) \\ &= \sum_{i=1}^{2} \left(\vartheta_i(\Xi_i\mathbf{K} + \Xi_i^- G_1)\right) \bar{\chi}(t) + M_2 e_\epsilon(t) \end{aligned} \tag{11}$$

where $\varrho(t) = \left[\bar{\chi}^T(t), e_\epsilon^T(t)\right]^T$, $e_\epsilon(t) = \epsilon(t) - \hat{\epsilon}(t)$. Ξ_i is a particular diagonal matrix in which each diagonal component is either 0 or 1, and $\Xi_i + \Xi_i^- = I$. $\mathbf{L}(G)$ is a symmetric polyhedron, that is $\mathbf{L}(G) = \{\bar{\chi} : |G_l\bar{\chi}| \le 1\}$, G_l denotes the lth row of matrix G. ϑ_i is known positive constants with $\vartheta_1 + \vartheta_2 = 1$.

Substituting the saturated input (11) into the extended system (7), one can be deduced as

$$\begin{aligned} \dot{\bar{\chi}}(t) = &\left(\mathcal{A}^* + \sum_{i=1}^{2} \vartheta_i \mathcal{B}^* \left(\Xi_i\mathbf{K} + \Xi_i^- G_1\right)\right) \bar{\chi}(t) \\ &+ \mathcal{C}^* \tilde{h}(\bar{\chi}(t), t) + \bar{\mathcal{C}} y_d(t) \end{aligned} \tag{12}$$

Define $\tilde{\aleph}(t) = \hat{\aleph}(t) - \aleph^*$. From (5), (9) and (10), we can obtain

$$\begin{aligned} \dot{e}_\epsilon(t) = &\left(M_1 + \mathbf{L}\mathcal{B}^* M_2\right) e_\epsilon(t) + \mathbf{L}\mathcal{C}^* \tilde{h}(\bar{\chi}(t), t) \\ &+ \sum_{i=1}^{2} \vartheta_i \mathbf{L}\mathcal{B}^* \Xi_i^- (G_1 - \mathbf{K})\bar{\chi}(t) \\ &+ \tilde{\aleph}(t)\Psi(\hat{\epsilon}(t)) + \aleph^* \left[\Psi(\hat{\epsilon}(t)) - \Psi(\epsilon(t))\right] \end{aligned} \tag{13}$$

Furthermore, by combing closed-loop system (12) with the error dynamics (13), it is possible to be inferrd that

$$\begin{aligned} \dot{\varrho}(t) = &\begin{bmatrix} \Gamma_{11} & \mathcal{B}^* M_2 \\ \Gamma_{21} & M_1 + \mathbf{L}\mathcal{B}^* M_2 \end{bmatrix} \varrho(t) + \begin{bmatrix} \mathcal{C}^* \\ \mathbf{L}\mathcal{C}^* \end{bmatrix} \tilde{h}(x(t), t) \\ &+ \begin{bmatrix} 0 \\ I \end{bmatrix} \times \left\{\tilde{\aleph}(t)\Psi(\hat{\epsilon}(t)) + \aleph^* \left[\Psi(\hat{\epsilon}(t)) - \Psi(\epsilon(t))\right]\right\} \\ &+ \begin{bmatrix} \bar{\mathcal{C}} \\ 0 \end{bmatrix} y_d \end{aligned} \tag{14}$$

where

$$\begin{cases} \Gamma_{11} = \mathcal{A}^* + \sum_{i=1}^{2} \vartheta_i \mathcal{B}^* \left(\Xi_i\mathbf{K} + \Xi_i^- G_1\right) \\ \Gamma_{21} = \sum_{i=1}^{2} \vartheta_i \mathbf{L}\mathcal{B}^* \Xi_i^- (G_1 - \mathbf{K}) \end{cases}$$

For the sake of achieving dynamical performance, some assumptions are needed.

Assumption 1: The activation function $\Psi(.)$ is assumed to satisfy the following inequality

$$\left(\Psi(\epsilon) - \Psi\left(\hat{\epsilon}\right)\right)^T \left(\Psi(\epsilon) - \Psi\left(\hat{\epsilon}\right)\right) \le e_\epsilon^T(t)\Pi_\epsilon^T \Pi_\epsilon e_\epsilon(t) \tag{15}$$

where $\Pi_\epsilon > 0$ is a known matrix.

Assumption 2: The disturbance $\sigma_2(t)$ satisfies the inequality $\sigma_2^T(t)\sigma_2(t) \le \sigma_{2h}$, where $\sigma_{2h} > 0$ is a positive constant.

IV. DYNAMICAL PERFORMANCE ANALYSIS AND ANGULAR VELOCITY CONSTRAINT

The next two theorems that follow in this part will cover the dynamical characteristics of closed-loop systems (12) and the estimate error system of disturbances (13).

Theorem 1: For the augmented closed-loop systems (12) and the disturbance estimation error (13), assume that matrices $P_2 > 0$, $Q_1 = P_1^{-1} > 0$ and V_i, $i = 1, 2, 3$ are found such that the following inequality

$$\begin{bmatrix} \Phi_{11} & \Phi_{12} & \bar{\mathcal{C}} & V_3\mathcal{C}^* & 0 & 0 \\ * & \Phi_{22} & 0 & 0 & V_3\mathcal{C}^* & P_2 \\ * & * & -\varpi_1^2 I & 0 & 0 & 0 \\ * & * & * & -\varpi_2^2 I & 0 & 0 \\ * & * & * & * & -\varpi_3^2 I & 0 \\ * & * & * & * & * & -\bar{\aleph}^{-1} \end{bmatrix} < 0 \tag{16}$$

with

$$\begin{cases} \Phi_{11} = sym\left(\mathcal{A}^* Q_1 + \vartheta_i \mathcal{B}^* \Xi_i V_1 + \vartheta_i \mathcal{B}^* \Xi_i^- V_2\right) + Q_1 \\ \Phi_{22} = sym\left(P_2 M_1 + V_3 \mathcal{B}^* M_2\right) + P_2 + \Pi_\epsilon^T \Pi_\epsilon + \varpi_4^{-2} I \\ \Phi_{12} = \mathcal{B}^* M_2 + \left(\vartheta_i V_3 \mathcal{B}^* \Xi_i^- (V_2 - V_1)\right)^T \end{cases}$$

is solvable, where $\varpi_i > 0, i = 1, 2, 3, 4$ are designed parameters.

Meanwhile, the adaptive adjustment rate of $\hat{\aleph}(t)$ is chosen as

$$\dot{\hat{\aleph}}(t) = \zeta P_2 \hat{\epsilon}(t)\sigma^T(\hat{\epsilon}(t)) - \|\hat{\epsilon}(t)\|\hat{\aleph}(t) \tag{17}$$

where $\zeta > 0$ is a known constant. Then the augmented system (14) can be guaranteed to be stable and the state $\varrho(t)$ converges into a compact set $\Omega_{\varrho(t)}$, where

$$\Omega_{\varrho(t)} = \left\{\varrho(t) : \|\varrho(t)\| \le \frac{\sqrt{\varpi_1^2 y_d^2 + \varpi_2^2 + \varpi_3^2 + \kappa}}{\lambda_{\min}(P^*)}\right\}$$

Further, the correspond gains are given by $\mathbf{K} = V_1 Q_1^{-1}$, $\mathbf{L} = P_2^{-1} V_3$ and $G_1 = V_2 Q_1^{-1}$.

Proof: Design the following Lyapunov functions as

$$\begin{aligned} \Theta_1(\bar{\chi}(t), t) = &\bar{\chi}^T(t) P_1 \bar{\chi}(t) \\ &+ \frac{1}{\lambda_1^2} \int_0^t \left[\|\Pi\bar{\chi}\|^2 - \|\tilde{h}(\bar{\chi}, \tau)\|^2\right] d\tau \end{aligned} \tag{18}$$

and

$$\Theta_2(e_\epsilon(t), t) = e_\epsilon^T(t) P_2 e_\epsilon(t) + tr\left\{\tilde{\aleph}^T(t)\tilde{\aleph}(t)\right\} \tag{19}$$

From (12), one can be inferred that

$$\begin{aligned} \dot{\Theta}_1 = &\bar{\chi}^T(t)\Bigg(sym\Bigg(\mathcal{A}^{*T} P_1 + P_1 \sum_{i=1}^{2} \vartheta_i \mathcal{B}^* (\Xi_i\mathbf{K} \\ &+ \Xi_i^- G_1)\Bigg)\Bigg)\bar{\chi}(t) + 2\bar{\chi}^T(t) P_1 \bar{\mathcal{C}} y_d \\ &+ 2\bar{\chi}^T(t) P_1 \mathcal{C}^* \tilde{h}(\bar{\chi}(t)) + 2\bar{\chi}^T(t) P_1 \mathcal{B}^* M_2 e_\epsilon(t) \\ &+ \frac{1}{\lambda_1}\left[\|\Pi\bar{\chi}\|^2 - \|\tilde{h}(\bar{\chi}, \tau)\|^2\right] \end{aligned}$$

$$\leq \bar{\chi}^T(t)\Big(sym\Big(\mathcal{A}^{*T}P_1+\varpi_1^{-2}P_1\mathcal{C}^*\mathcal{C}^{*T}P_1+P_1\sum_{i=1}^{2}\vartheta_i\mathcal{B}^*\times\left(\Xi_i\mathbf{K}+\Xi_i^-G_1\right)+\varpi_2^{-2}P_1\bar{\mathcal{C}}\bar{\mathcal{C}}^TP_1\Big)+\frac{1}{\lambda_1^2}\Pi^T\Pi\Big)\bar{\chi}(t)+2\bar{\chi}^T(t)P_1\mathcal{B}^*M_2e_\epsilon(t)+\varpi_1^2\tilde{h}^T(\bar{\chi}(t))\tilde{h}(\bar{\chi}(t))+\varpi_2^2y_d^2(t) \tag{20}$$

Based on (13) and (17), we have

$$\dot{\Theta}_2\leq e_\epsilon^T(t)\left(sym\left(P_2M_1+P_2\mathbf{L}\mathcal{B}^*M_2\right)\right)e_\epsilon(t)+2e_\epsilon^T(t)\left(P_2\sum_{i=1}^{2}\vartheta_i\mathbf{L}\mathcal{B}^*\Xi_i^-(G_1-\mathbf{K})\right)\bar{\chi}(t)+2\epsilon^T(t)P_2\tilde{\aleph}(t)\sigma(\hat{\epsilon})-2\|\hat{\epsilon}(t)\|tr\left\{\tilde{\aleph}^T(t)\hat{\aleph}(t)\right\}+e_\epsilon^T(t)\left(P_2\tilde{\aleph}P_2\Pi_\epsilon^T\Pi_\epsilon\right)e_\epsilon(t) \tag{21}$$

Due to

$$2tr\left\{\tilde{\aleph}^T(t)\hat{\aleph}(t)\right\}\geq\|\tilde{\aleph}(t)\|_F^2-\|\aleph^*\|_F^2, \tag{22}$$

$$2\epsilon^T(t)P_2\tilde{\aleph}(t)\sigma(\hat{\epsilon}(t))\leq\sqrt{\frac{2\theta_hn_\epsilon}{\lambda_{\min}(M_2^TM_2)}}\|P_2\|\cdot\left(\zeta\sqrt{n_\epsilon}\|P_2\|+\sqrt{tr(\bar{\aleph})}\right) \tag{23}$$

where $\bar{\aleph}$ is the upper bound of optimal weight $\aleph^*$ and meets the inequality $\aleph^{*T}\aleph^*\leq\bar{\aleph}$.

Then, (21) is deduced as

$$\dot{\Theta}_2\leq e_\epsilon^T(t)\left(sym(P_2M_1+P_2\mathbf{L}\mathcal{B}^*M_2)\right)e_\epsilon(t)+2e_\epsilon^T(t)\left(P_2\sum_{i=1}^{2}\vartheta_i\mathbf{L}\mathcal{B}^*\Xi_i^-(G_1-\mathbf{K})\right)\bar{\chi}(t)+e_\epsilon^T(t)\left(P_2\bar{\aleph}P_2+\Pi_\epsilon^T\Pi_\epsilon\right)e_\epsilon(t)+\sqrt{\frac{2\theta_hn_\epsilon}{\lambda_{\min}(M_2^TM_2)}}\|P_2\|\left(\zeta\sqrt{n_\epsilon}\|P_2\|+\sqrt{tr(\bar{\aleph})}\right)+2\|\hat{\epsilon}(t)\|\|\aleph^*\|_F^2 \tag{24}$$

Notice that

$$2\|\hat{\epsilon}(t)\|\|\aleph^*\|_F^2\leq\varpi_4^{-2}e_\epsilon(t)^Te_\epsilon(t)+\sqrt{\frac{4\theta_h}{\lambda_{\min}(M_2^TM_2)}}tr\left\{\bar{\aleph}\right\}+\varpi_4^2\left(tr\left\{\bar{\aleph}\right\}\right)^2 \tag{25}$$

By integrating (20) with (24), one has

$$\dot{\Theta}_1+\dot{\Theta}_2=\bar{\chi}^T(t)\Big(sym\Big(\mathcal{A}^{*T}P_1+P_1\sum_{i=1}^{2}\vartheta_i\mathcal{B}^*\times\left(\Xi_i\mathbf{K}+\Xi_i^-G_1\right)+\varpi_1^{-2}P_1\mathcal{C}^*\mathcal{C}^{*T}P_1+\varpi_2^{-2}P_1\bar{\mathcal{C}}\bar{\mathcal{C}}^TP_1\Big)+\frac{1}{\lambda_1^2}\Pi^T\Pi\Big)\bar{\chi}(t)+e_\epsilon^T(t)\left(sym(P_2M_1+P_2\mathbf{L}\mathcal{B}^*M_2)+\Pi_\epsilon^T\Pi_\epsilon+P_2\bar{\aleph}P_2+\varpi_4^{-2}I\right)e_\epsilon(t)+2e_\epsilon^T(t)\times\left(M_2^T\mathcal{B}^{*T}P_1+P_2\sum_{i=1}^{2}\vartheta_i\mathbf{L}\mathcal{B}^*\Xi_i^-(G_1-\mathbf{K})\right)\times\bar{\chi}(t)+\varpi_1^2y_d^2+\varpi_2^2+\kappa\leq\max_{i\in\{1,2\}}\left\{\varrho^T(t)\begin{bmatrix}\Omega_{11i}&\Omega_{12i}\\*&\Omega_{22i}\end{bmatrix}\varrho(t)\right\}+\varpi_1^2y_d^2+\varpi_2^2+\varpi_3^2+\kappa \tag{26}$$

where

$$\kappa=\sqrt{\frac{2\theta_hn_w}{\lambda_{\min}(M_2^TM_2)}}\|P_2\|\left(\zeta\sqrt{n_w}\|P_2\|+\sqrt{tr(\bar{\aleph})}\right)+\sqrt{\frac{4\theta_h}{\lambda_{\min}(M_2^TM_2)}}tr\{\bar{\aleph}\}+\varpi_3^2\left(tr\{\bar{\aleph}\}\right)^2$$

and

$$\begin{cases}\Omega_{11i}=sym\Big(\mathcal{A}^{*T}P_1+P_1\sum_{i=1}^{2}\vartheta_i\mathcal{B}^*\left(\Xi_i\mathbf{K}+\Xi_i^-G_1\right)+\varpi_1^{-2}P_1\mathcal{C}^*\mathcal{C}^{*T}P_1+\varpi_2^{-2}P_1\bar{\mathcal{C}}\bar{\mathcal{C}}^TP_1\Big)+\frac{1}{\lambda_1^2}\Pi^T\Pi\\ \Omega_{22i}=sym(P_2M_1+P_2\mathbf{L}\mathcal{B}^*M_2)+\Pi_w^T\Pi_w+P_2\bar{\aleph}P_2+\varpi_4^{-2}I\\ \Omega_{21i}=\left(\vartheta_iP_2\mathbf{L}\mathcal{B}^*\Xi_i^-(G_1-\mathbf{K})\right)^T+P_1\mathcal{B}^*M_2\end{cases}$$

Based on the Schur complement, by pre- and post-multiplying (16) with $diag\{Q_1^{-1};I;I;I;I;I\}$, and defining $V_1=\mathbf{K}Q_1$, $V_2=G_1Q_1$ and $V_3=P_2\mathbf{L}$, it can be seen that (21) implies

$$[\Omega_{11i},\Omega_{12i};\Omega_{21i},\Omega_{22i}]<diag\{-P_1,-P_2\}$$

Then (26) is transformed as

$$\dot{\Theta}_1+\dot{\Theta}_2\leq-\varrho^T(t)P^*\varrho(t)+\varpi_1^2y_d^2+\varpi_2^2+\varpi_3^2+\kappa \tag{27}$$

where $P^*=diag\{P_1,P_2\}$. It is easy to deduce that once $\varrho^T(t)P^*\varrho(t)>\varpi_1^2y_d^2+\varpi_2^2+\varpi_3^2+\kappa$ is true, $\dot{\Theta}_1+\dot{\Theta}_2<0$ can be generated.

As a result, for any variables $e_\epsilon(t)$ and $\bar{\chi}(t)$, it is inferred that

$$\varrho^T(t)P^*\varrho(t)\leq\max\left\{\varrho^T(0)P^*\varrho(0),\varpi_1^2y_d^2+\varpi_2^2+\varpi_3^2+\kappa\right\} \tag{28}$$

is valid for any $t\geq0$. It is further demonstrated that the augmented system (14) is stable and that $\varrho(t)$ will converge towards the intended compact set $\Omega_{\varrho(t)}$.

Theorem 2: Considering given parameters $\varpi_i, i=1,2,3,4$ and $\zeta>0$, For given parameters, if there are matrices $P_2>0$, $Q_1=P_1^{-1}$ and $V_i, i=1,2,3$ such that (16) and the following inequalities

$$\begin{bmatrix} Q_1 & Q_1\mathcal{D}^{*T}_1 \\ * & \left(\pi^{-1}y_d^2\right)I \end{bmatrix} \geq 0 \tag{29}$$

and

$$\begin{bmatrix} Q_1 & Q_1N^T \\ * & \left(\pi^{-1}x_{2d}^2\right)I \end{bmatrix} \geq 0 \tag{30}$$

are solvable, the augmented closed-loop system (14) can be proved as stability, and the dynamic tracking error will converge to zero, that is $lim_{t\to\infty}y(t) = y_d$. Meanwhile, the angular velocity constraint $|x_2(t)| \leq x_{2d}$ can be guaranteed, even in the presence of exogenous disturbances. Therein, $N = [0\ 1\ 0\ 0\ 0\ 0]$, $\pi = \max\left\{\varrho^T(0)P^*\varrho(0), \varpi_1^2y_d^2 + \varpi_2^2 + \varpi_3^2 + \kappa\right\}$, x_{2d} is the expected signal of angular velocity. In addition, the gain matrices are computed via $\mathbf{K} = V_1Q_1^{-1}$, $\mathbf{L} = P_2^{-1}V_3$ and $G_1 = V_2Q_1^{-1}$.

Proof: The stability of the composite closed-loop system (14) may be ensured by resolving (16) and (17), which is analogous to the proof of Theorem 1. As for the system output $y(t)$ and the second component $x_2(t)$ of state variable, we can get

$$\begin{aligned} y^2(t) &= \bar{\chi}^T(t)\mathcal{D}^{*T}\mathcal{D}^*\bar{\chi}(t) \\ x_2^2(t) &= \bar{\chi}^T(t)N^TN\bar{\chi}(t) \end{aligned} \tag{31}$$

From the equality (30) and (31), it is not difficult to deduce

$$\begin{aligned} \mathcal{D}^{*T}\mathcal{D}^* &\leq \pi^{-1}y_d^2P_1 \\ N^TN &\leq \pi^{-1}x_{2d}^2P_1 \end{aligned} \tag{32}$$

Based on (32) and (33), we can achieve that

$$\begin{aligned} y^2(t) &\leq \pi^{-1}y_d^2\bar{\chi}^T(t)P_1\bar{\chi}(t) \leq y_d^2 \\ x_2^2(t) &\leq \pi^{-1}x_{2d}^2\bar{\chi}^T(t)P_1\bar{\chi}(t) \leq x_{2d}^2 \end{aligned} \tag{33}$$

On one hand, notice that the item $\int_0^t e(\tau)d\tau$ is a component of $\varrho(t)$, the variable $\int_0^t e(\tau)d\tau$ necessarily converge into the set $\Omega_{\varrho(t)}$ when $t \to +\infty$. Meanwhile, due to the inequality $y^2(t) \leq y_d^2$ in (33), $e(t) \leq 0$ can be guaranteed for any $t \geq 0$. So $\int_0^t e(\tau)d\tau$ is monotone decreasing function. In short, $lim_{t\to\infty}\int_0^t e(\tau)d\tau$ must exist. On the other hand, based on assumptions 1, 2 and (28), it is not hard to derive that $x(t)$, $e_\epsilon(t)$ and $\sigma_2(t)$ are bounded. Further, $\dot{e}(t)$ is also bounded. So the uniformly continuous of $e(t)$ can be guaranteed. Based on the Barbalat's Lemma, the dynamical tracking satisfies $\lim_{t\to\infty} y(t) = y_d$. In addition, it is easy to induce from (33) that the angular velocity $x_2(t)$ also can be compressed within the limit of x_{2d}, that is $|x_2(t)| \leq x_{2d}$.

Remark 2: In this paper, it is assumed that irregular disturbances can be represented by an exogenous model (5), where $\aleph^* \in \mathbb{R}^{5\times5}$ refers to the optimal weight vector and $\Psi(\star)$ is the activation function. Please note that adjustable parameters $\hat{\aleph}(t)$ in (9) are those parameters that can be tuned by using the designed algorithm. That is, different parameter values can be selected to optimize the performance of the model in different datasets or applications. These parameters are usually not fixed but can be adjusted as required. Typical examples include learning rates, weight decay coefficients, etc. In this article, the parameters are adjusted by using the designed adaptive algorithm (17).

V. SIMULATION RESULTS

In this section, the simulations of a typical single-link manipulator system driven by PMSM are carried out. Concretely, the following Figure 1 shows the flow diagram of the controller design. The desired tracking signal and the angular velocity constraint are $y_d = 25$, $x_{2d} = 30$, respectively. Similarly with [9], the parameters of the system are given in Table 1.

TABLE 1. Parameters and variables of the single-link flexible manipulator drive.

Parameter	Description	Value
K	Spring elasticity coefficient	$1.15kg\cdot m^2$
I	Moment of inertia	$2.3\times10^{-2}kg\cdot m^2$
B	Coefficient of viscous friction	$4.7\times10^{-2}m/rad$
J	Rotor inertia	$2.26\times10^{-2}kg\cdot m^2$
l_p	Number of pole pairs	6
ψ	Rotor fiux linkage	$8.1\times10^{-2}Wb$
R_s	Stator resistance	0.6Ω
L	Stator inductance	2.5×10^{-4}
M	Link and load mass	19.39kg
l	Link length	1.56m
g	Gravity coefficient	9.8N/kg
r	Reduction ratio	1

From (4), the system matrices of the single-link manipulators are easy to be inferred that

$$\mathcal{A} = \begin{bmatrix} 0 & 1 & 0 & 0 & 0 \\ 50 & -0.047 & -50 & 0 & 0 \\ 0 & 0 & 0 & 1 & 0 \\ 150 & 0 & -150 & 0 & 21.504 \\ 0 & 0 & 0 & -0.486 & -2400 \end{bmatrix}$$

$$\mathcal{B} = \begin{bmatrix} 0 \\ 0 \\ 0 \\ 0 \\ 40 \end{bmatrix}, \mathcal{C} = \begin{bmatrix} 0 \\ 1 \\ 0 \\ 0 \\ 0 \end{bmatrix}, \mathcal{D}^T = \begin{bmatrix} 1 \\ 0 \\ 0 \\ 0 \\ 0 \end{bmatrix}$$

In the following, as for different types of disturbances, simulation results are presented to verify the designed algorithm.

Model 1 (Attenuated Harmonic (AH) Disturbances): As the signal is transmitted, the signal usually continues to be attenuated and eventually remains at a smaller amplitude. So the modeling of AH disturbances has great significance. In this part, the parameters are chosen as

$$M_1 = \begin{bmatrix} -0.25 & -1.3 \\ 1 & -0.01 \end{bmatrix}, \quad M_2 = \begin{bmatrix} -3 & 2 \end{bmatrix}$$

$$\aleph^* = \begin{bmatrix} -0.5 & 0.5 \\ -0.004 & 0.45 \end{bmatrix}, \quad \epsilon(t) = \begin{bmatrix} tanh(t) \\ arctan(t) \end{bmatrix}$$

and the candidate value of V_3 is preselected as

$$V_3 = \begin{bmatrix} 0 & 1.3547 & 11.2113 & 45.1257 & 0 & 0 \\ 0 & 0.0325 & -43.4435 & -30.2578 & 0 & 0 \end{bmatrix}$$

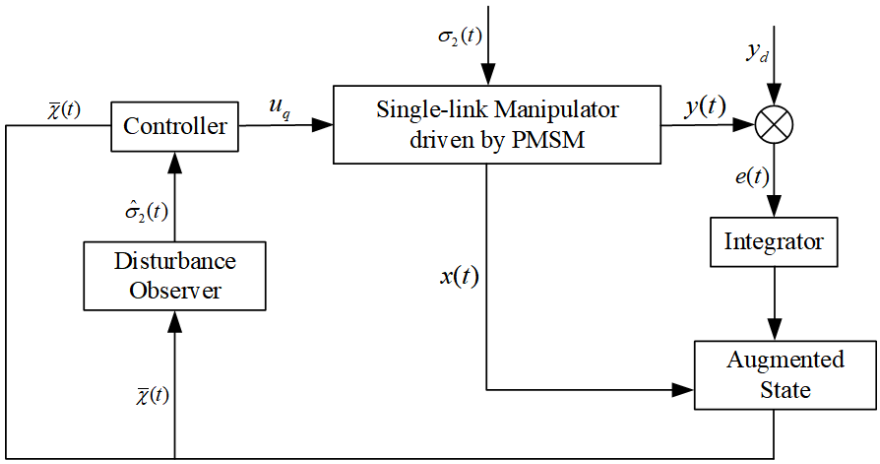

FIGURE 1. The flow chart of controller design.

Then, by setting the parameters $\varpi_1 = \varpi_2 = \varpi_3 = 0.8$, the control gain $\mathbf{K_I}$ and $\mathbf{K_P}$, the observer gain $\mathbf{L}$ as well as the vector G_1 are computed as

$$\mathbf{K_I} = 1.0412$$
$$\mathbf{K_P} = \begin{bmatrix} 11.8058 & 6.3810 & 8.4406 & -2.1992 & 5.4268 \end{bmatrix}$$
$$\mathbf{L} = 10^{-4} \begin{bmatrix} 0 & 0.0076 & 0.0789 & 0.0375 & 0 & 0 \\ 0 & -0.0038 & -0.1802 & -0.04721 & 0 & 0 \end{bmatrix}$$
$$G_1 = \begin{bmatrix} -0.3095 & 0.2943 & 0.2068 & -0.1175 & 0.0274 & -0.0871 \end{bmatrix}$$

Assume that the initial values of the augmented states are displayed as $x_0 = [2, -2, -3, 0, 0]^T$ and $\epsilon_0 = [-0.2, 1]^T$, respectively. The trajectories of the system states are described in Figure 2, which shows the favorable stability. Figure 3 depicts the estimation value, the estimation error, and the attenuated harmonic disturbances, demonstrating the validity of the developed DO. Figure 4 and Figure 5 illustrate the saturated input and the tracking trajectory of desired signal y_d, revealing that the input saturation and dynamical tracking are adequate. Figure 6 shows the dynamic trajectory of the neural network weight.

From the Figure 2 and 5, the curves have large fluctuation in the simulation results of the system state and output trajectory. On one hand, the selection of the initial values and the step size leads to the large fluctuations in the simulation curve. By selecting more appropriate initial values, the fluctuation will abate. On the other hand, due to the presence of irregular disturbances in the controlled system, the designed disturbance observer (see (9) for details) can not track the irregular disturbances accurately, especially at the beginning. So it will cause huge fluctuations in the system state and output curves. After a period of time, the designed disturbance observer can accurately estimate for unknown disturbances, the system state and output curves will also be smoothed out.

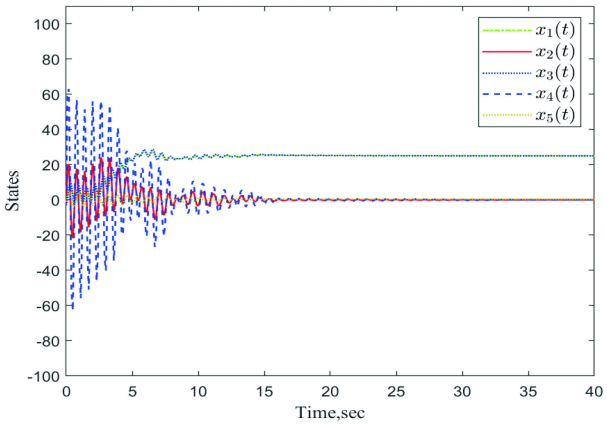

FIGURE 2. State trajectories of the single-link manipulator with AH disturbances.

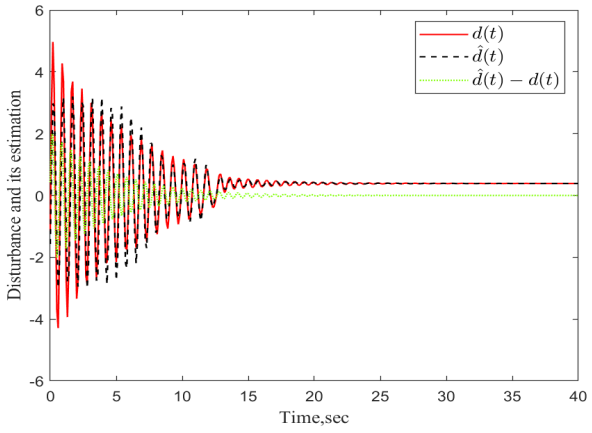

FIGURE 3. AH disturbances, its estimation and estimation error.

Model 2 (Irregular Triangular Wave (ITW) Disturbance): ITW signals are usually caused by the change of the rating and characteristics of some parts with the applicable conditions, and this disturbance is difficult to be described by linear exogenous systems. So it is necessary to develop

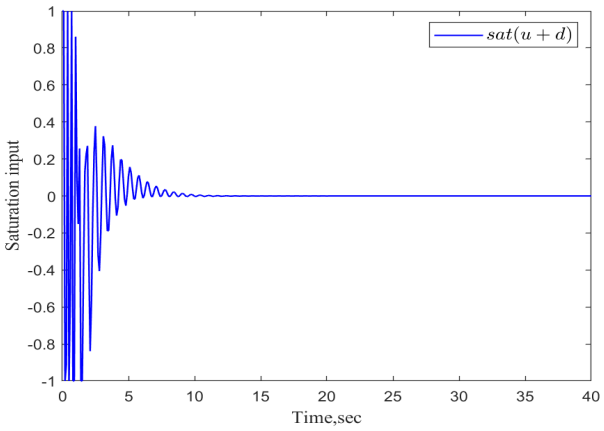

FIGURE 4. Dynamics of the saturated control input with AH disturbances.

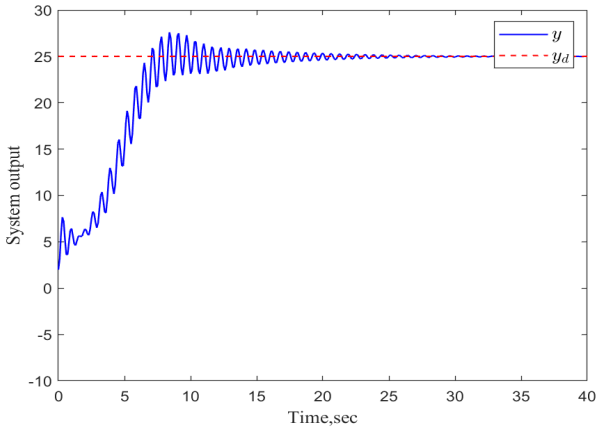

FIGURE 5. Dynamics of the system output with AH disturbances and its desired trajectory.

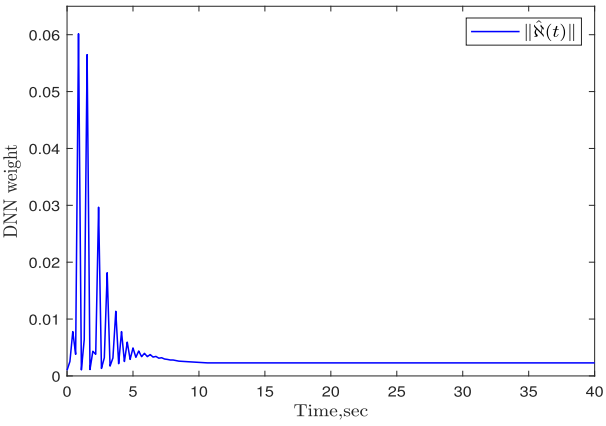

FIGURE 6. Dynamic trajectory of the DNN weight.

effective models to estimate such irregular disturbances. The parameters are selected as

$$M_1 = \begin{bmatrix} -0.45 & 8 \\ -10 & 0 \end{bmatrix}, \quad M_2 = \begin{bmatrix} 0.43 & -2 \end{bmatrix}$$
$$\aleph^* = \begin{bmatrix} -0.3 & 5 \\ -0.04 & 0.45 \end{bmatrix}$$

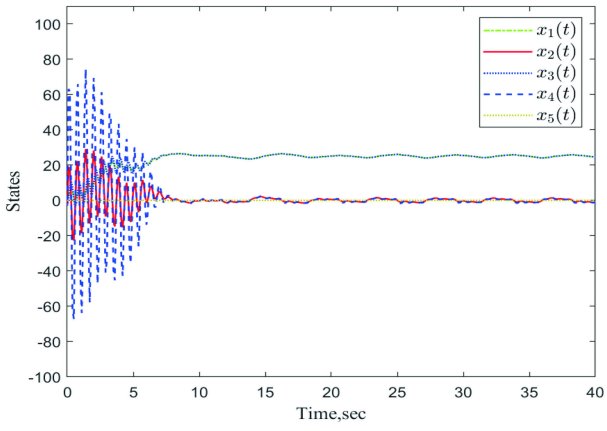

FIGURE 7. State trajectories of the single-link manipulator with ITW disturbances.

$$\epsilon(t) = \begin{bmatrix} \dfrac{1}{1+e^{-0.2t}} \\ \dfrac{1}{1+e^{-0.2t}} \end{bmatrix} t \geq 0, \quad \epsilon(t) = \begin{bmatrix} -2.5 \\ -2.5 \end{bmatrix} t < 0$$

The gains $\mathbf{K_I}$, $\mathbf{K_P}$, $\mathbf{L}$ and G_1 can be calculated via completing BLMIs (16) as long as $\varpi_1 = \varpi_2 = \varpi_3 = 1$.

$$\mathbf{K_I} = 0.2118$$
$$\mathbf{K_P} = \begin{bmatrix} 2.9548 & 1.7032 & -2.2306 & -0.7244 & 0.4502 \end{bmatrix}$$
$$\mathbf{L} = 10^{-5} \begin{bmatrix} 0 & 0.0889 & 0.3847 & 0.7526 & 0 & 0 \\ 0 & -0.4894 & -0.3337 & -0.5529 & 0 & 0 \end{bmatrix}$$
$$G_1 = \begin{bmatrix} -0.0112 & 0.0438 & 0.0105 & -0.0198 \\ & & & 0.0046 \quad -0.0110 \end{bmatrix}$$

Suppose that the initial values are set as $x_0 = [5, -3, 2, 0, 0]^T$ and $\epsilon_0 = [-0.2, 1]^T$. The tracking signal is designed as $y_d = 25$. Figure 7 is the dynamics of the state of the single-link manipulator system. The trajectory of ITW disturbance and its estimates are demonstrated in Figure 8. Figure 9 and Figure 10 reflect the saturated input and the tracking result of desired signal y_d, respectively. As shown in Figure 9, it should be noted, the vertical coordinate takes values in the range of -1 and 1. The system input signal fluctuates from the range of -0.4 to 0.4. In general, such input fluctuations have little effect on the motor. In Figure 11, the trajectory of the neural network weight dynamics is presented.

Model 3 (White Noice (WN) Disturbances): It is well known WN disturbances are one of the most common disturbances in electronic products. Specifically, the parameters are selected as

$$M_1 = \begin{bmatrix} 0.25 & 0.1 \\ -8 & -0.5 \end{bmatrix}, \quad M_2 = \begin{bmatrix} 5 & -0.3 \end{bmatrix}$$
$$\aleph^* = \begin{bmatrix} -0.5 & 0.8 \\ 3 & 0.5 \end{bmatrix},$$
$$\epsilon(t) = \begin{bmatrix} \dfrac{e^{0.2t} - e^{-0.2t}}{e^{0.2t} + e^{-0.2t}} \\ \dfrac{e^{0.2t} - e^{-0.2t}}{e^{0.2t} + e^{-0.2t}} \end{bmatrix}$$

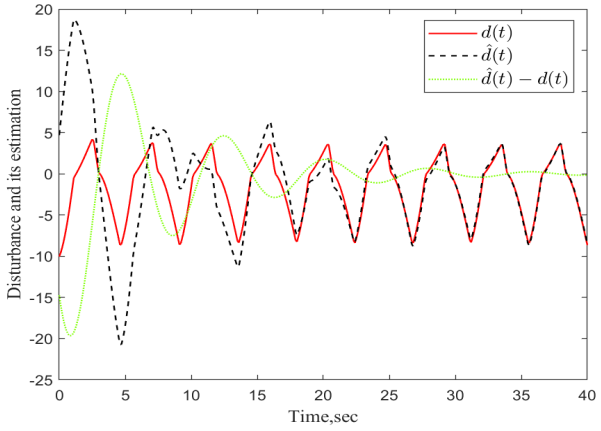

FIGURE 8. ITW disturbances, its estimation and estimation error.

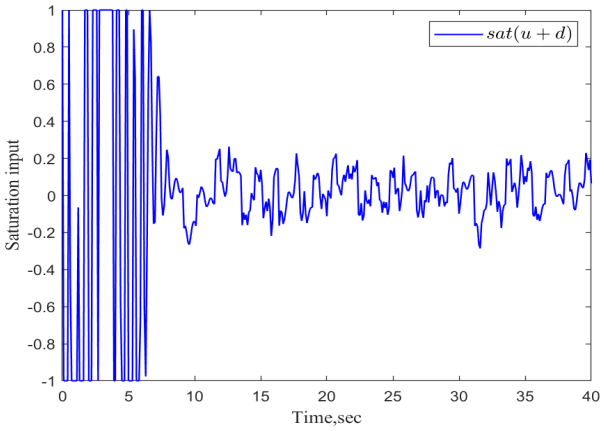

FIGURE 9. Dynamics of the saturated control input with ITW disturbances.

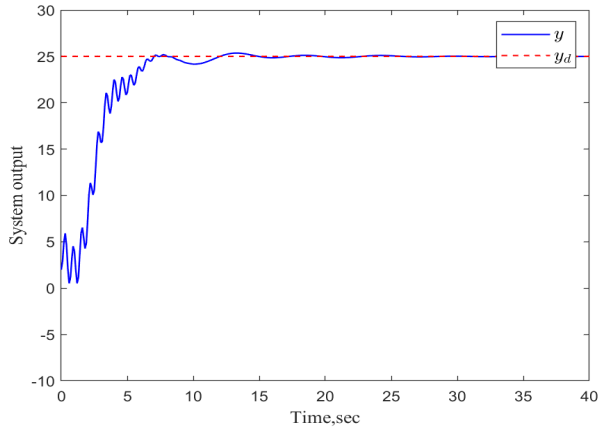

FIGURE 10. Dynamics of the system output with ITW disturbances and its desired trajectory.

Select $\varpi_1 = \varpi_2 = 1, \varpi_3 = 0.8$, the gains $\mathbf{K_I}$, $\mathbf{K_P}$ and $\mathbf{L}$ can be obtained from solving BLMIs (16) as

$$\mathbf{K_I} = 0.4813$$
$$\mathbf{K_P} = \begin{bmatrix} 11.5539 & 6.2645 & -8.3510 & -2.1939 & 0.9476 \end{bmatrix}$$
$$\mathbf{L} = 10^{-3} \begin{bmatrix} 0 & 0.0012 & 0.0036 & 0.0034 & 0 & 0 \\ 0 & -0.0011 & -0.1008 & -0.0730 & 0 & 0 \end{bmatrix}$$

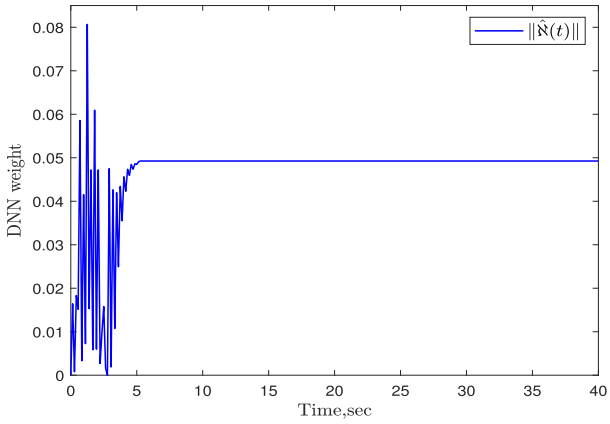

FIGURE 11. Dynamic trajectory of the DNN weight.

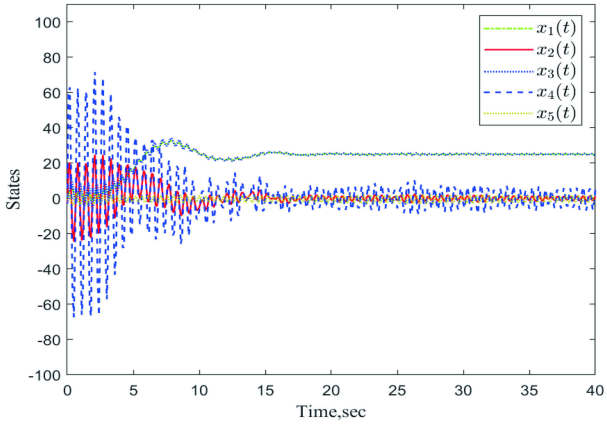

FIGURE 12. State trajectories of the single-link manipulator with WN disturbances.

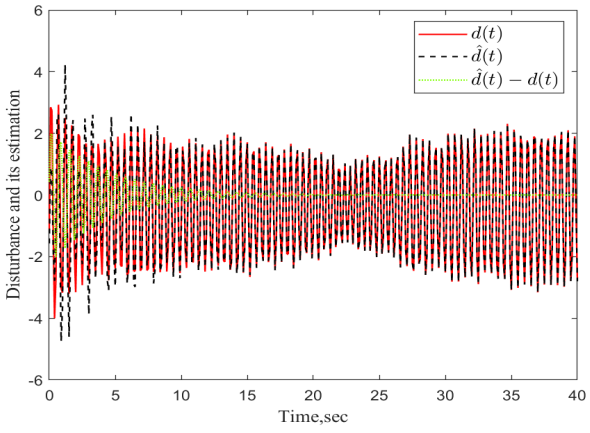

FIGURE 13. WN disturbances, its estimation and estimation error.

$$G_1 = \begin{bmatrix} -0.0422 & 0.1506 & 0.0664 & -0.0687 \\ & & & 0.0019 \quad -0.0361 \end{bmatrix}$$

The initial values may be set as $x_0 = [2, -2, -3, 0, 0]^T$ and $\epsilon_0 = [2, 1]^T$. The dynamics of the states are exhibited in Figure 12. Figure 13 shows the tracks of WN disturbances and their corresponding estimates. In addition, Figures. 14 and 15 plot the dynamics of the saturated input and the system

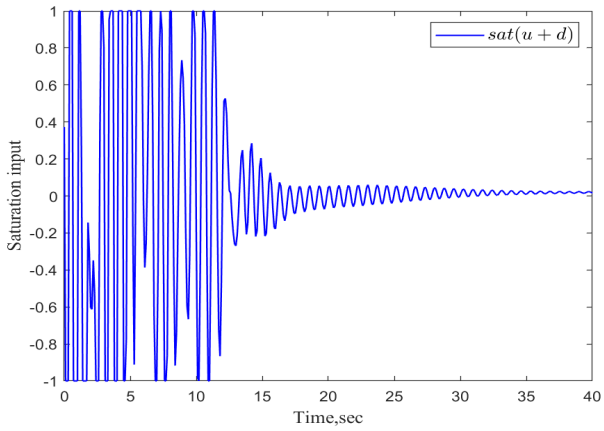

FIGURE 14. Dynamics of the saturated control input with WN disturbances.

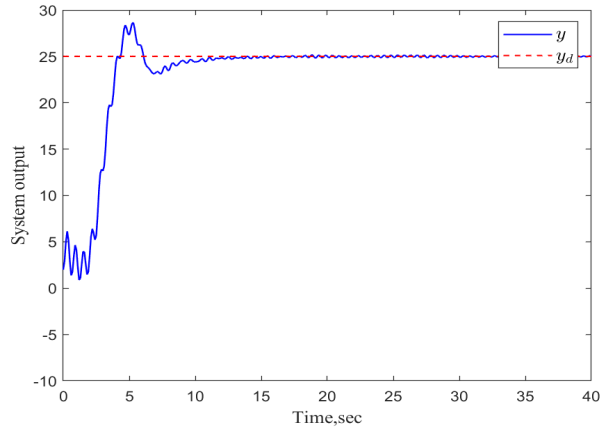

FIGURE 15. Dynamics of the system output with WN disturbances and its desired trajectory.

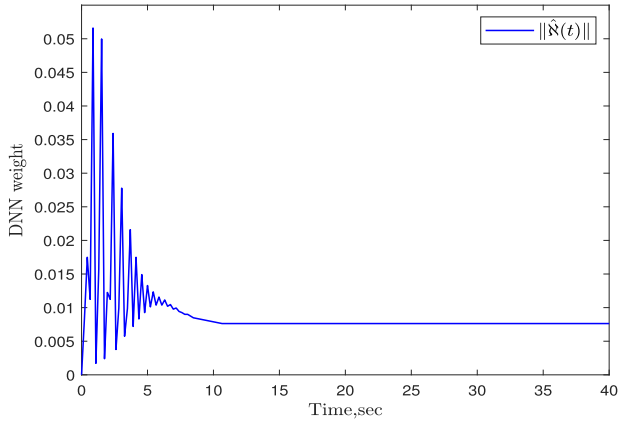

FIGURE 16. Dynamic trajectory of the DNN weight.

output, respectively, which further reveals the satisfactory dynamic tracking performance and the rationality of the proposed controller. The trajectory of the neural network weight dynamics is revealed in Figure 16.

VI. CONCLUSION

This study successfully applies an efficient active anti-disturbance control algorithm to the single-link manipulator systems driven by PMSM. A novel DO-based adaptive feedback control input is proposed to monitor those irregular disturbances. The polytopic description of input saturation is utilized to construct a composite anti-disturbance controller using the estimated value of disturbances. Based on convex optimization theory, relevant proofs are given to guarantee stability and disturbance suppression performance. Meanwhile, both the favorable dynamic tracking and the restriction of angular velocity have also been realized. Ultimately, it can be seen from the simulation results on a single-link manipulator that the suggested strategy is efficient in terms of the desired control performances. As a final note, when dealing with multi-input multi-output systems suffering from more types of unknown disturbances and faults, a multi-source complex anti-disturbance control framework with better performance will be considered in our further research. Furthermore, the implementation and application of related algorithms in more diverse practical scenarios will be an interesting topic for our future work.

REFERENCES

[1] H. Gao, W. He, C. Zhou, and C. Sun, "Neural network control of a two-link flexible robotic manipulator using assumed mode method," *IEEE Trans. Ind. Informat.*, vol. 15, no. 2, pp. 755–765, Feb. 2019.
[2] B. Xu, "Composite learning control of flexible-link manipulator using NN and DOB," *IEEE Trans. Syst., Man, Cybern., Syst.*, vol. 48, no. 11, pp. 1979–1985, Nov. 2018.
[3] W. He, F. Kang, L. Kong, Y. Feng, G. Cheng, and C. Sun, "Vibration control of a constrained two-link flexible robotic manipulator with fixed-time convergence," *IEEE Trans. Cybern.*, vol. 52, no. 7, pp. 5973–5983, Jul. 2022.
[4] F. Dong, B. Yu, X. Zhao, S. Chen, and H. Liu, "Constraint-following servo control for the trajectory tracking of manipulator with flexible joints and mismatched uncertainty," *Machines*, vol. 9, no. 9, p. 202, Sep. 2021.
[5] Z. Liu, X. Tang, and L. Wang, "Research on the dynamic coupling of the rigid-flexible manipulator," *Robot. Comput.-Integr. Manuf.*, vol. 32, pp. 72–82, Apr. 2015.
[6] Q. Meng, X. Lai, Z. Yan, and M. Wu, "Tip position control and vibration suppression of a planar two-link rigid-flexible underactuated manipulator," *IEEE Trans. Cybern.*, vol. 52, no. 7, pp. 6771–6783, Jul. 2022.
[7] Y. Li, S. S. Ge, Q. Wei, T. Gan, and X. Tao, "An online trajectory planning method of a flexible-link manipulator aiming at vibration suppression," *IEEE Access*, vol. 8, pp. 130616–130632, 2020.
[8] J. S. Yeon and J. H. Park, "Practical robust control for flexible joint robot manipulators," in *Proc. IEEE Int. Conf. Robot. Autom.*, May 2008, pp. 3377–3382.
[9] Z. Zhang, X. Liu, J. Yu, and H. Yu, "Time-varying disturbance observer based improved sliding mode single-loop control of PMSM drives with a hybrid reaching law," *IEEE Trans. Energy Convers.*, vol. 14, no. 8, pp. 1416–1426, May 2022.
[10] T. Li, X. Liu, and H. Yu, "Backstepping nonsingular terminal sliding mode control for PMSM with finite-time disturbance observer," *IEEE Access*, vol. 9, pp. 135496–135507, 2021.
[11] Q. Yang, H. Yu, X. Meng, and Y. Shang, "Neural network dynamic surface position control of n-joint robot driven by PMSM with unknown load observer," *IET Control Theory Appl.*, vol. 16, no. 12, pp. 1208–1226, 2022.
[12] J. Daafouz, G. Garcia, and J. Bernussou, "Robust control of a flexible robot arm using the quadratic d-stability approach," *IEEE Trans. Control Syst. Technol.*, vol. 6, no. 4, pp. 524–533, Jul. 1998.
[13] C. Lin and T. Lin, "An H_∞ design approach for neural net-based control schemes," *IEEE Trans. Autom. Control*, vol. 46, no. 10, pp. 1599–1605, Oct. 2001.
[14] Y. Sun, S. Tong, and Y. Liu, "Adaptive backstepping sliding mode H_∞ control of static var compensator," *IEEE Trans. Contr. Syst. Technol.*, vol. 19, no. 5, pp. 1178–1185, Sep. 2011.

[15] Q. Wei, H. Li, and F.-Y. Wang, "A novel parallel control method for continuous-time linear output regulation with disturbances," *IEEE Trans. Cybern.*, vol. 53, no. 6, pp. 3760–3770, Jun. 2023, doi: 10.1109/TCYB.2021.3128231.
[16] W.-H. Chen, "Disturbance observer based control for nonlinear systems," *IEEE/ASME Trans. Mechatronics*, vol. 9, no. 4, pp. 706–710, Dec. 2004.
[17] X. Yao, J. H. Park, L. Wu, and L. Guo, "Disturbance-observer-based composite hierarchical antidisturbance control for singular Markovian jump systems," *IEEE Trans. Autom. Control*, vol. 64, no. 7, pp. 2875–2882, Jul. 2019.
[18] Y. Yi, L. Guo, and H. Wang, "Constrained PI tracking control for output probability distributions based on two-step neural networks," *IEEE Trans. Circuits Syst. I, Reg. Papers*, vol. 56, no. 7, pp. 1416–1426, Jul. 2009.
[19] Y. Yi, W. X. Zheng, and L. Guo, "Improved results on statistic information control with a dynamic neural network identifier," *IEEE Trans. Circuits Syst. II, Exp. Briefs*, vol. 60, no. 11, pp. 816–820, Nov. 2013.
[20] Y. Yi, W. X. Zheng, and B. Liu, "Adaptive anti-disturbance control for systems with saturating input via dynamic neural network disturbance modeling," *IEEE Trans. Cybern.*, vol. 52, no. 6, pp. 5290–5300, Jun. 2022.
[21] Y. Zhang, J. Sun, H. Liang, and H. Li, "Event-triggered adaptive tracking control for multiagent systems with unknown disturbances," *IEEE Trans. Cybern.*, vol. 50, no. 3, pp. 890–901, Mar. 2020.
[22] H. Pan, W. Sun, H. Gao, and X. Jing, "Disturbance observer-based adaptive tracking control with actuator saturation and its application," *IEEE Trans. Autom. Sci. Eng.*, vol. 13, no. 2, pp. 868–875, Apr. 2016.
[23] J. Sun, J. Yi, and Z. Pu, "Fixed-time adaptive fuzzy control for uncertain nonstrict-feedback systems with time-varying constraints and input saturations," *IEEE Trans. Fuzzy Syst.*, vol. 30, no. 4, pp. 1114–1128, Apr. 2022.
[24] Y. Wei, W. X. Zheng, and S. Xu, "Anti-disturbance control for nonlinear systems subject to input saturation via disturbance observer," *Syst. Control Lett.*, vol. 85, pp. 61–69, Nov. 2015.
[25] M. Chen, H. Wang, and X. Liu, "Adaptive practical fixed-time tracking control with prescribed boundary constraints," *IEEE Trans. Circuits Syst. I, Reg. Papers*, vol. 68, no. 4, pp. 1716–1726, Apr. 2021.
[26] A. Bemporad, "Reference governor for constrained nonlinear systems," *IEEE Trans. Autom. Control*, vol. 43, no. 3, pp. 415–419, Mar. 1998.
[27] B. Ren, S. S. Ge, K. P. Tee, and T. H. Lee, "Adaptive neural control for output feedback nonlinear systems using a barrier Lyapunov function," *IEEE Trans. Neural Netw.*, vol. 21, no. 8, pp. 1339–1345, Aug. 2010.
[28] X. Yao, L. Wu, and L. Guo, "Disturbance-observer-based fault tolerant control of high-speed trains: A Markovian jump system model approach," *IEEE Trans. Syst., Man, Cybern., Syst.*, vol. 50, no. 4, pp. 1476–1485, Apr. 2020.
[29] J. Yang, H. Cui, S. Li, and A. Zolotas, "Optimized active disturbance rejection control for DC–DC buck converters with uncertainties using a reduced-order GPI observer," *IEEE Trans. Circuits Syst. I, Reg. Papers*, vol. 65, no. 2, pp. 832–841, Feb. 2018.

WENYE ZHOU received the B.Sc. degree from the Wenzheng College, Soochow University, Suzhou, China, in 2017. He is currently pursuing the master's degree in control engineering with Yangzhou University. His current research interests include robust control, dynamic surface control, and anti-disturbance control.

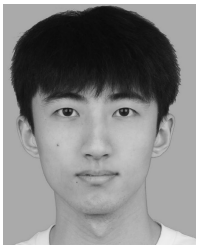

CHEN LIN received the B.Sc. degree from the Guangzhou College, South China University of Technology, Guangzhou, China, in 2017. He is currently pursuing the master's degree in control engineering with Yangzhou University. His current research interests include event-triggered control and anti-disturbance control.

YANG YI received the M.Sc. degree in information engineering from Yangzhou University, Yangzhou, China, in 2005, and the Ph.D. degree in automation from Southeast University, Nanjing, China, in 2009. From 2012 to 2013, he was a Visiting Scientist with the School of Computing, Engineering and Mathematics, University of Western Sydney, Penrith, NSW, Australia. He is currently a Professor with the College of Information Engineering, Yangzhou University. He has published more than 60 papers in journals and conferences. His current research interests include stochastic systems, intelligent systems, and anti-disturbance control.